

Current-induced magnetization switching in MgO barrier based magnetic tunnel junctions with
CoFeB/Ru/CoFeB synthetic ferrimagnetic free layer

Jun HAYAKAWA^{1,2}, Shoji IKEDA², Young Min LEE², Ryutaro SASAKI²,
Toshiyasu MEGURO², Fumihiro MATSUKURA², Hiromasa TAKAHASHI^{1,2},
and Hideo OHNO²

*1. Hitachi,Ltd.,Advanced Research Laboratory,1-280 Higashi-koigakubo, Kokubunji-shi, Tokyo
185-8601, Japan*

*2. Laboratory for Nanoelectronics and Spintronics, Research Institute of Electrical Communication,
Tohoku University, 2-1-1 Katahira, Aoba-ku, Sendai 980-8577, Japan*

(Received;

We report the intrinsic critical current density (J_{c0}) in current-induced magnetization switching and the thermal stability factor ($E/k_B T$, where E , k_B , and T are the energy potential, the Boltzmann constant, and temperature, respectively) in MgO based magnetic tunnel junctions with a $\text{Co}_{40}\text{Fe}_{40}\text{B}_{20}(2\text{nm})/\text{Ru}(0.7\text{-}2.4\text{nm})/\text{Co}_{40}\text{Fe}_{40}\text{B}_{20}(2\text{nm})$ synthetic ferrimagnetic (SyF) free layer. We show that J_{c0} and $E/k_B T$ can be determined by analyzing the average critical current density as a

function of coercivity using the Slonczewski's model taking into account thermal fluctuation. We find that high antiferromagnetic coupling between the two CoFeB layers in a SyF free layer results in reduced J_{c0} without reducing high $E/k_B T$.

KEYWORDS: current-induced magnetization switching, synthetic free layer, magnetic tunnel junction, MgO barrier, CoFeB

E-mail: j-hayaka@rd.hitachi.co.jp

Spin-polarized currents exert torque on a magnetization that can switch the magnetization direction once the current density becomes sufficiently high.^{1,2)} Such a current-induced magnetization switching (CIMS) at reduced current density has been demonstrated in a number of magnetic tunnel junctions (MTJs).³⁾⁻⁵⁾ In particular, CoFeB/MgO/CoFeB MTJs have been shown to exhibit high tunnel magnetoresistance (TMR) ratios together with CIMS.⁶⁾⁻⁹⁾ In order to use this system for magnetic random access memories, however, further reduction of the critical current density (J_c) while maintaining a high thermal stability factor over 40 ($E/k_B T$, where E , k_B , and T are the energy potential, the Boltzmann constant, and temperature, respectively) is required to satisfy the nonvolatility over 10 years. Meeting this requirement with a conventional single ferromagnetic free layer patterned into a nanometer-scale shape appears to be not easy as the thermal stability degrades as the dimension is reduced. Synthetic ferrimagnetic (SyF) free layer has been investigated as an alternative to the single free layer because the SyF structure consisting of two or more ferromagnetic layers separated by a non-magnetic spacer such as Ru film is expected to provide high volume to withstand thermal fluctuations.¹⁰⁾⁻¹²⁾ In current-perpendicular-to-plane giant magnetoresistance (CPP-GMR) nanopillars, where only a small magnetoresistance ratio can be obtained, CIMS with SyF free layers were investigated and J_c , measured using a dc current sweep, was reported to be lower than that of conventional single free layer MTJs¹³⁾. However, intrinsic critical current density J_{c0} , which we define in the following, and $E/k_B T$ of such a nanopillar, either CPP-GMR or MTJ, with

a SyF free layer have not been investigated so far.

In this letter, we focus on MgO barrier based MTJs with a $\text{Co}_{40}\text{Fe}_{40}\text{B}_{20}/\text{Ru}/\text{Co}_{40}\text{Fe}_{40}\text{B}_{20}$ SyF free layer and investigate J_{c0} and $E/k_B T$. The J_{c0} and $E/k_B T$ are shown to be able to be determined by analyzing the average critical current density (J_c^{ave}) as a function of coercivity using the Slonczewski's model taking into account thermal fluctuation. Thus obtained J_{c0} and $E/k_B T$ are in good agreement with those obtained by J_c^{ave} versus $\ln(\tau_p/\tau_0)$ plots, where τ_p and τ_0 represent the current pulse duration and inverse of the precession frequency. The J_{c0} is defined as the critical current density at the inverse precession frequency.

Figure 1 (a) is a schematic diagram of the MTJ pillar we fabricated. MTJ films were deposited on SiO_2/Si substrates by using RF magnetron sputtering with a base pressure of 10^{-9} Torr. The order of the film layers was, starting from the substrate side, $\text{Ta}(5) / \text{Ru}(50) / \text{Ta}(5) / \text{NiFe}(5) / \text{MnIr}(8) / \text{CoFe}(4) / \text{Ru}(0.8) / \text{Co}_{40}\text{Fe}_{40}\text{B}_{20}(5) / \text{MgO} (0.9-1.0) / \text{Co}_{40}\text{Fe}_{40}\text{B}_{20}(2) / \text{Ru}(t_{Ru}) / \text{Co}_{40}\text{Fe}_{40}\text{B}_{20}(2) / \text{Ta}(5) / \text{Ru}(5)$ (in nm). The Ru spacers varying in thickness from 0.7 nm to 2.4 nm were formed by using a slide mask shutter during sputtering. All nano-scaled junctions were fabricated using an electron-beam lithography process. Figure 1 (b) shows scanning electron microscopy images of rectangular-shaped MTJ pillars with the dimension of $80 \times 160 \text{ nm}^2$ (top image) and $80 \times 240 \text{ nm}^2$ (bottom one). The completed MTJs were annealed at temperature of 300°C for 1 h in a 10^{-6} Torr vacuum under a magnetic field of 4 kOe. The TMR loops of the MTJs were measured at room

temperature using a four-probe method with dc bias and magnetic field of up to 1 kOe. CIMS was evaluated by measuring resistance by 50 μ A-step current pulses with the pulse duration (τ_p) ranging from 100 μ s to 1 s. The thermal stability factor $E/k_B T$ was obtained from the slope of the average critical current density J_c^{ave} versus $\ln(\tau_p/\tau_0)$ plot, in addition to the method proposed in this paper. The current direction is defined as positive when the electrons flow from the top (free) to the bottom (pin) layer.

In order to determine the magnetic exchange coupling energy J_{ex} between the two CoFeB ferromagnetic layers as a function of t_{Ru} in the CoFeB(2)/Ru(t_{Ru})/CoFeB(2) structure, we prepared separately a structure, SiO₂/Si substrate / Ta(5) / Ru (50) / Ta(5) / MgO(0.9) / CoFeB(2) / Ru(t_{Ru}) / CoFeB(2) / Ta(5), which is cut into a rectangular with the dimension of 1 x 3 mm² for magneto-optical Kerr effect measurements. Figure 2 (a) plots magnetic exchange coupling energy J_{ex} between the two CoFeB ferromagnetic layers as a function of t_{Ru} . Inset shows the expanded view of the range from $t_{\text{Ru}} = 1.0$ nm to 3.0 nm. The highest antiferromagnetic coupling energy of 0.17 mJ/m² is obtained at $t_{\text{Ru}} \sim 0.6$ nm. We also see oscillations in the magnitude of J_{ex} ; the second peak is located at $t_{\text{Ru}} = 1.2$ nm and the third at $t_{\text{Ru}} = 2.4$ nm. Negative J_{ex} and $J_{\text{ex}} = 0$ correspond to the antiferromagnetic and ferromagnetic coupling, respectively. Therefore, the J_{ex} is found to oscillate from ferromagnetic to antiferromagnetic and back as reported earlier¹⁴⁾, which originates from the Ruderman-Kittel-Kasuya-Yosida (RKKY)-type coupling typically found in Co/Ru/Co multilayers.¹⁵⁾

Figure 2(b) shows the coercivity H_c obtained from the TMR measurements under magnetic field as a function of t_{Ru} of the nanoscaled MTJs. The H_c strongly depends on the t_{Ru} and greater the J_{ex} higher the H_c .

Figures 3 (a) and (b) show the magnetic field hysteresis loop (R-H loop) and the resistance versus pulsed current ($R-I_p$) with $\tau_p = 10$ ms of a 80×160 nm 2 MTJ with a CoFeB(2)/Ru(0.7)/CoFeB(2) SyF free layer. The Ru thickness of 0.7 nm corresponds to the highest antiferromagnetic coupling energy. The TMR ratio is 90%, which is comparable to the one reported for an MTJ with a 2-nm CoFeB single free layer.⁴ The $R - I_p$ curves were measured under an applied magnetic field of -32 Oe along the direction of the pin CoFeB layer to compensate the offset field (see Fig. 3 (a)) arising primarily from the stray fields of the edge of the patterned SyF pin layer. The current density required to switch the magnetization from parallel (anti-parallel) to anti-parallel (parallel) shown in Fig. 3 (b) is $J_c^{P \rightarrow AP} = 6.8 \times 10^6$ A/cm 2 ($J_c^{AP \rightarrow P} = -6.8 \times 10^6$ A/cm 2); the average critical current density (J_c^{ave}), defined as $(|J_c^{P \rightarrow AP}| + |J_c^{AP \rightarrow P}|)/2$, is 6.8×10^6 A/cm 2 . Figure 3 (c) plots J_c^{ave} as a function of $\ln(\tau_p/\tau_0)$ for τ_p from 100 μ s to 1 s for the same MTJs shown in Fig. 3 (a) and (b). Based on Eq. (1) shown later, the slope of this plot reveals the thermal stability factors $E/k_B T$ to be 67. By extrapolating J_c to $\ln(\tau_p/\tau_0)$ of 0 which corresponds to $\tau_p = 1$ ns, we obtain the intrinsic critical current density (J_{c0}) of 8.7×10^6 A/cm 2 .

Figure 4 (a) plots J_c^{ave} as a function of $1/H_c$ (inverse of the coercivity H_c) of all the MTJs

investigated in this study, with varying Ru spacers from 0.7 nm to 2.4 nm. Here, all J_c^{ave} were measured with a pulse current of 1 s duration. We have noticed that (1) J_c^{ave} can be categorized into three groups, depending on the strength of the magnetic coupling energy J_{ex} shown in Fig. 2, and (2) within each group J_c^{ave} increases linearly with H_c . The black symbols ($t_{Ru} = 0.7$ and 0.9 nm), white symbols ($t_{Ru} = 1.5, 1.7$ and 1.9 nm), and hatched square symbols ($t_{Ru} = 2.2$ and 2.4 nm) correspond to the Ru spacer thickness for the first antiferromagnetic coupling, the ferromagnetic coupling between the second and third anti-ferromagnetic coupling, and the third antiferromagnetic coupling, respectively. Hereafter, we call them Group I, Group II, and Group III, respectively.

We now show that the J_{c0} and $E/k_B T$ can be obtained by analyzing the measured J_c^{ave} versus H_c using the following Slonczewski's model^{1),16)} taking into account the thermal activated nature of the magnetization switching. The relevant equations are;^{17),18)}

$$J_c = J_{c0} \{1 - (k_B T/E) \ln(\tau_p/\tau_0)\}, \quad (1)$$

$$J_{c0} = \alpha \gamma e M_s t (H_{ext} \pm H_k \pm H_d) / \mu_B g, \quad (2)$$

$$E = M_s V H_k / 2, \quad (3)$$

$$g = P / [2(1+P^2 \cos \theta)], \quad (4)$$

where α is the Gilbert damping coefficient, γ the gyromagnetic constant, e the elementary charge, t the thickness of the free layer, H_{ext} the external magnetic field, H_k the in-plane uniaxial magnetic anisotropy, M_s the saturation magnetization of free layer, V the volume of free layer and H_d the

out-of-plane magnetic anisotropy induced by the demagnetization field. θ is 0 for the parallel configuration and π for anti-parallel. In the following, we assume that our magnetic cell has a uni-axial anisotropy and a single magnetic domain, and hence $H_k \approx H_c$, because we are dealing with nanoscale structures. Since $H_d \gg H_k, H_{ext}$, we obtain the average J_{c0} (J_{c0}^{ave}), and J_c^{ave} , which is a function of H_c , as,

$$J_{c0}^{ave} \approx \alpha \gamma e M_s t H_d (g^{(P>AP)} + g^{(AP>P)}) / \mu_B g^{(P>AP)} g^{(AP>P)} \quad (5)$$

$$J_c^{ave} = J_{c0}^{ave} [1 - (2k_B T / M_s V) \ln(\tau_p / \tau_0) / H_c] \quad (6)$$

As seen in Fig. 4 (a), the measured J_c^{ave} are inversely proportional to H_c within each group (solid lines). This shows that eq. (6) is a good approximation describing our results. By extrapolating $1/H_c$ to zero in Fig. 4 (a), we can then obtain J_{c0}^{ave} , given by Eq. (5), as 9.4×10^6 A/cm² for Group I, 1.57×10^7 A/cm² for Group II, and 1.65×10^7 A/cm² for Group III. Thus determined J_{c0}^{ave} value for Group I is in good agreement with the value obtained from the J_c^{ave} versus $\ln(\tau_p / \tau_0)$ plot of Fig. 3 (c) (8.7×10^6 A/cm²). This also shows that $\tau_0 = 1$ ns is a reasonable value for the inverse precession frequency. We speculate that the reduction of J_{c0}^{ave} for the MTJs of Group I may be related to spin-accumulation; two antiferromagnetically coupled CoFeB layers separated by a non-magnetic Ru layer whose thickness is much thinner than the spin diffusion length¹⁹⁾ is known to enhance the spin accumulation at the CoFeB and Ru interface.^{20),21)} Spin accumulation can increase the efficiency of spin-torque acting on the CoFeB free layer and contribute to the reduction of critical current

density. Clearly more work is needed to clarify the mechanism.

Next, we compare the thermal stability factors $E/k_B T$ between MTJs categorized into three groups from Fig. 4 (a). The slope of J_c^{ave} vs. $1/H_c$ is given by $-J_{c0}^{ave}(2k_B T/M_s V) \ln(\tau_p/\tau_0)$ according to eq. (6). Because $E/k_B T = M_s V H_c / 2k_B T$ the factor obtained by dividing the slope by $-J_{c0}^{ave}(\ln(\tau_p/\tau_0)) \times H_c$ should yield the $E/k_B T$, where τ_p and τ_0 are 1 s and 1 ns, respectively. We calculate the factors $(2k_B T/M_s V)^{-1} \times H_c$ for all the MTJs shown in Fig. 4 (a) as summarized in Fig. 4 (b), where we employ the J_{c0}^{ave} obtained by extrapolating $1/H_c$ to zero in Fig. 4 (a). We notice that the MTJs having a large antiferromagnetic coupling energy (Group I) exhibit smaller J_{c0} values together with higher $(2k_B T/M_s V)^{-1} \times H_c$, hence higher $E/k_B T$, than those in other groups (Group II and Group III).

In conclusion, we have determined intrinsic critical current density (J_{c0}) for current-induced magnetization switching and the thermal stability factor ($E/k_B T$) of MgO barrier based MTJs with $\text{Co}_{40}\text{Fe}_{40}\text{B}_{20}(2\text{nm})/\text{Ru}(0.7\text{-}2.4\text{nm})/\text{Co}_{40}\text{Fe}_{40}\text{B}_{20}(2\text{nm})$ synthetic ferromagnetic (SyF) free layers. The J_{c0} and $E/k_B T$ are shown to be able to be determined using J_c^{ave} versus $1/H_c$ curves. High antiferromagnetic coupling between the two CoFeB ferromagnetic layers is found to result in a reduced J_{c0} together with a high thermal stability factor $E/k_B T$ over 60.

This work was supported by the IT-program of the Research Revolution 2002 (RR2002): “Development of Universal Low-power Spin Memory”, Ministry of Education, Culture, Sports, Science and Technology of Japan.

References

- 1) J. C. Slonczewski: *J. Magn. & Magn. Mater.* **159** (1996) L1.
- 2) L. Berger: *Phys. Rev. B* **54** (1996) 9353.
- 3) H. Kubota, A. Fukushima, Y. Ootani, S. Yuasa, K. Ando, H. Maehara, K. Tsunekawa, D. D. Djayaprawira, N. Watanabe, and Y. Suzuki: *Jpn. J. Appl. Phys.* **44** (2005) L1237.
- 4) J. Hayakawa, S. Ikeda, Y. M. Lee, R. Sasaki, F. Matsukura, T. Meguro, M. Takahashi, and H. Ohno: *Jpn. J. Appl. Phys.* **44** (2005) L1267.
- 5) Z. Diao, D. Apalkov, M. Pakala, Y. Ding, A. Panchula, and Y. Huai: *Appl. Phys. Lett.* **87** (2005) 232502.
- 6) S. Yuasa, T. Nagahama, A. Fukushima, Y. Suzuki, and K. Ando: *Nat. Mater.* **3** (2004) 868.
- 7) S. S. P. Parkin, C. Kaiser, A. Panchula, P. M. Rice, B. Hughes, M. Samant, and S.-H. Yang: *Nat. Mater.* **3** (2004) 862.
- 8) D. D. Djayaprawira, K. Tsunekawa, M. Nagai, H. Maehara, S. Yamagata, N. Watanabe, S. Yuasa, Y. Suzuki, and K. Ando: *Appl. Phys. Lett.* **86** (2005) 092502.
- 9) S. Ikeda, J. Hayakawa, Y. M. Lee, T. Tanikawa, F. Matsukura, and H. Ohno: *Jpn. J. Appl. Phys.* **44** (2005) L1442.
- 10) K. Inomata, T. Nozaki, N. Tezuka, and S. Sugimoto: *Appl. Phys. Lett.* **81** (2002) 310.
- 11) R. C. Sousa, Z. Zhang, and P. P. Freitas: *J. Appl. Phys.* **91** (2002) 7700.

12) Y. Saito, H. Sugiyama, and K. Inomata: *J. Appl. Phys.* **97** (2005) 10C914.

13) T. Ochiai, Y. Jiang, A. Hirohata, N. Tezuka, S. Sugimoto, K. Inomata: *Appl. Phys. Lett.* **86** (2005) 242506.

14) N. Wiese, T. Dimopoulos, M. Rührig, J. Wecker, H. Brückl, and G. Reiss: *Appl. Phys. Lett.* **85** (2004) 2020.

15) S. S. P. Parkin and D. Mauri: *Phys. Rev. B.* **44** (1991) 7131.

16) J. C. Slonczewski: *Phys. Rev. B.* **71** (2005) 02411.

17) R. H. Koch, J. A. Katine, and J. Z. Sun: *Phys. Rev. Lett.* **92** (2004) 088302.

18) D. Lacour, J. A. Katine, N. Smith, M. J. Carey, and J. R. Childress: *Appl. Phys. Lett.* **85** (2004) 4681.

19) K. Eid, R. Fonck, M. AlHaj Darwish, W. P. Pratt, Jr., and J. Bass: *J. Appl. Phys.* **91** (2002) 8102.

20) A. Fert, V. Cros, J.-M. Gerorge, J. Grollier, H. Jaffres, A. Hamzic, A. Vaures, G. Faini, J. Ben Youssef, and H. Le Gall: *cond-mat/0310737* (2003).

21) Y. Jiang, T. Nozaki, S. Abe, T. Ochiai, A. Hirohata, N. Tezuka, and K. Inomata: *Nat. Mater.* **3** (2004) 361.

Figure captions

Fig. 1. (a) Schematic drawing of the cross section of the MTJs. The thickness of the Ru spacer in the SyF layer varies from 0.7 to 2.4 nm. (b) Scanning electron microscopy image of the pillars.

Fig. 2. (a) Magnetic exchange coupling energy J_{ex} for CoFeB/Ru/CoFeB SyF layers with Ru spacers varying from 0 to 3 nm in thickness. Inset shows the expanded view of the plots ranging from $t_{Ru} = 1.0$ to 3.0 nm. (b) Coercivity (H_c) as a function of t_{Ru} in the nano-scaled MTJs with CoFeB/Ru/CoFeB SyF free layer.

Fig. 3. R-H loops (a), R- I_p loops at τ_p of 10 ms (b), and J_c^{ave} ($(J_c^{P>AP} - J_c^{AP>P})/2$) as functions of $\ln(\tau_p/\tau_0)$ (c) at room temperature for an MTJ with a CoFeB(2 nm)/Ru(0.7 nm)/CoFeB(2 nm) SyF free layer.

Fig. 4. J_c^{ave} as a function of $1/H_c$ (inverse of the H_c) (a), and $E/k_B T$ (b) for MTJs with SyF free layers having Ru spacers ranging from 0.7 to 2.4 nm. The plotted black symbols ($t_{Ru} = 0.7, 0.9$, and 1.2 nm), white symbols ($t_{Ru} = 2.2$ and 2.4 nm), and hatched square symbols ($t_{Ru} = 1.5, 1.7$, 1.9 nm) correspond to the Ru spacer thickness for the first/second antiferromagnetic coupling, the

ferromagnetic coupling between the second and third antiferromagnetic coupling, and the third antiferromagnetic coupling, respectively.

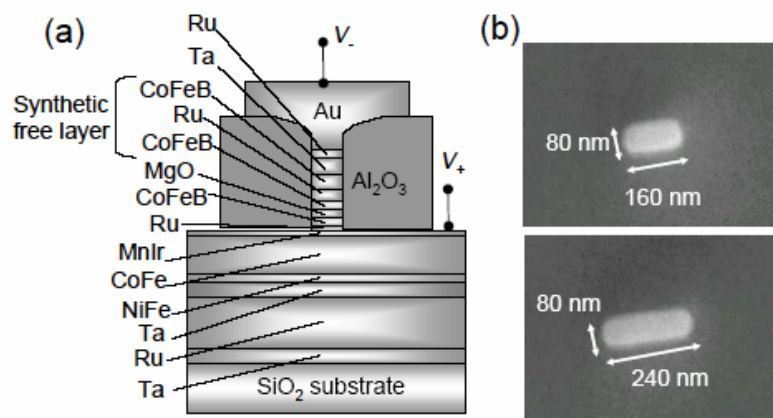


Figure 1 Hayakawa et al.

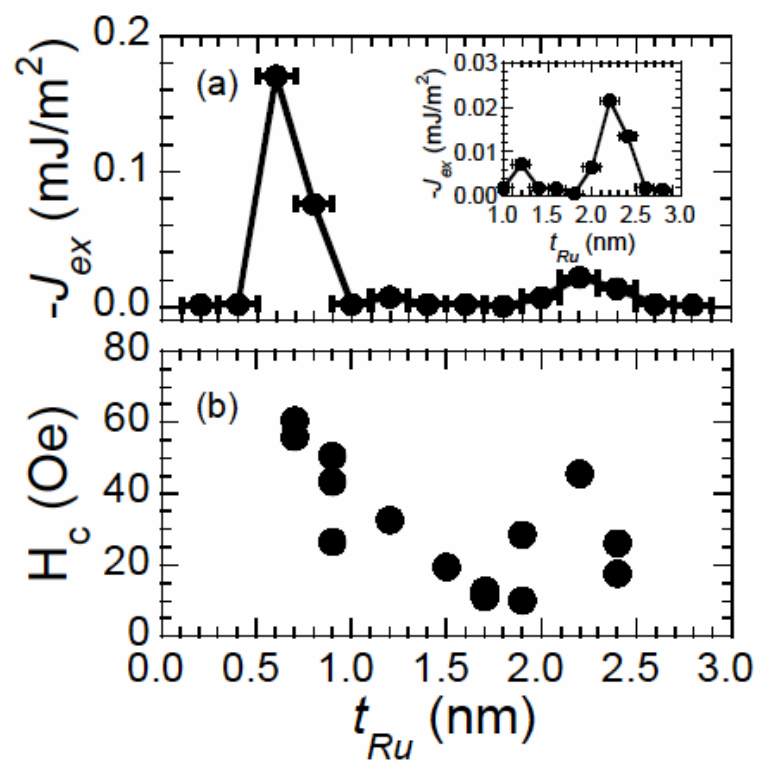


Figure 2 Hayakawa et al.

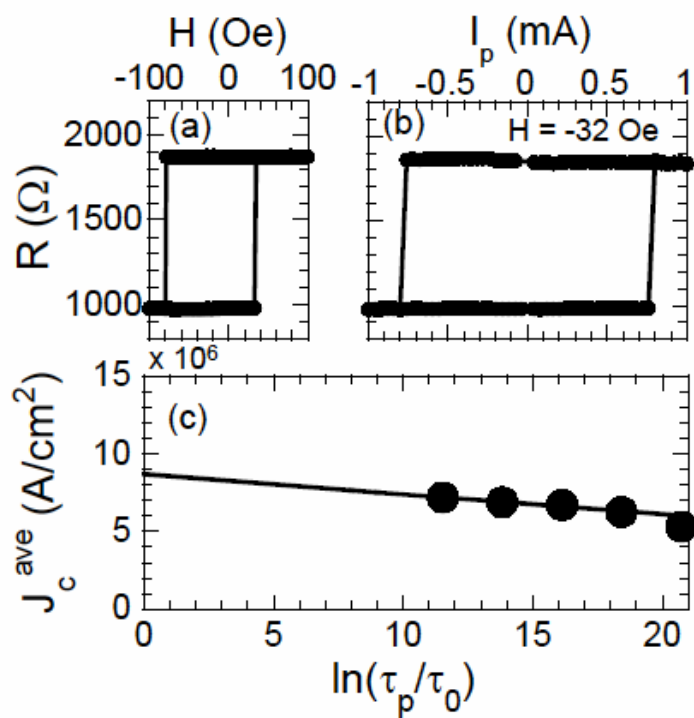


Figure 3 Hayakawa et al.

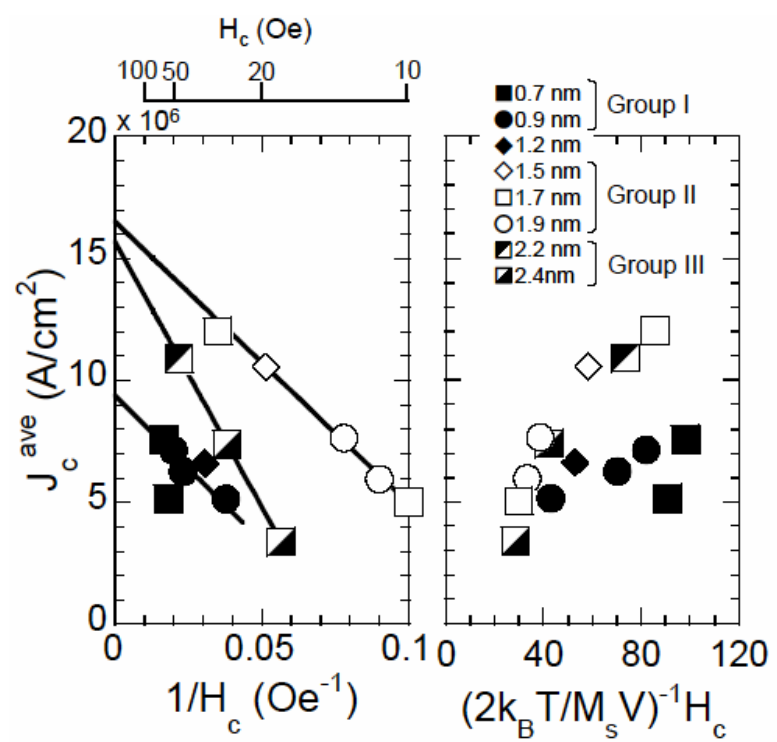


Figure 4 Hayakawa et al.